J Mater Sci (2007) 42:7316–7323
DOI 10.1007/s10853-006-1168-3

Microstructure and ferroelectric properties of soft-doped sol–gel derived PZT/SKN fibers

Ralf Hansch · Wolfgang Braue · Susanne Seifert · Dieter Sporn · Gerd Müller

Received: 12 March 2006 / Accepted: 20 October 2006 / Published online: 10 May 2007
© Springer Science+Business Media, LLC 2007

Abstract Sol–gel derived PZT/SKN fibers with a final composition of $0.98(PbO)_{1+z}(Zr_{0.53}Ti_{0.47})O_2$-0.02Sr$(K_{0.25}Nb_{0.75})O_3$ and a PbO content of z = +0.04 and +0.14 in the spinning sol were sintered at different temperatures. Fiber stoichiometry, phase content and microstructure as well as the physical properties of the fibers were investigated. A fully densified microstructure independent from the initial PbO content was obtained for fibers sintered at 950 °C or higher. Enhanced porosity was found only for fibers sintered at 900 °C. The densification of the fiber batches at the lower temperatures is dominated by solid state sintering, while liquid phase sintering is promoted by sintering at temperatures above 900 °C. TEM investigations confirmed the homogeneous nature of the PZT/SKN fibers devoid of compositional gradients. Typical dielectric permittivity is in the range of 650–1000. The ferroelectric hysteresis loops are well pronounced showing typical soft-doped behavior with remanent polarization values in the range of 15 and 34 $\mu C/cm^2$ and coercivities of about 1.9 V/μm.

R. Hansch (✉)
Landeskriminalamt NRW, SG51.1, Völklingerstrasse 49, 40221 Dusseldorf, Germany
e-mail: ju.bongartz@t-online.de

W. Braue
Materials Research Institute, German Aerospace Center (DLR), 51147 Cologne, Germany

S. Seifert
Ludwig-Thoma-Str., Wertingen, Germany

D. Sporn · G. Müller
Fraunhofer-Institut für Silicatforschung, Neunerplatz 2, 97082 Wuerzburg, Germany

Introduction

Multifunctional ceramic/polymer composites with integrated doped or undoped PZT fibers as the piezoactive constituent offer a high potential for sensoric and actoric applications [1–5]. Much effort has been directed towards the development of ultrasonic medical applications in the high frequency range as well as for the detection of forces, strains or vibrations [5–8].

Most preparation routes for these PZT-fibers are different compared to the processing of conventional PZT mixed oxide materials [9–12]. In terms of their densification characteristics PZT fibers differ from PZT bulk ceramics of the same nominal composition due to their significantly increased surface to volume ratio. This fact plays an important role for the understanding of the effects of the processing parameters upon the development of the fiber microstructure.

As reported, PZT fibers have been prepared from mixed-oxide powders, with fiber diameters in the range of 100–500 μm [13–17]. These rather thick fibers show very good piezoelectric properties with coupling coefficients k_t of about 55%; however, some applications of these fibers are limited due to their large diameters or limitations in fiber length. As an important advantage, these fibers provide easy handling similar to bulk ceramics prepared from mixed oxide powders.

In contrast, our research is focusing on thin sol–gel derived fibers in the system PZT–SrKNb according to a composition of a mixed oxide ceramic given by the company CeramTec [18, 19]. The sol–gel process accounts for small fiber diameters down to 20 μm as well as for the preparation of batches of several hundred single fibers up to 0.5 m in length. Furthermore, sintering temperatures can be kept comparably low due to the fact, that the elemental

distribution in the dried gel fiber is quite homogeneous. Due to the high surface/volume ratio of the fibers a careful control of the PbO partial pressure is required to compensate PbO losses and to achieve a 100% perovskitic yield. As shown in a previous paper [20] two different experimental techniques were pursued using (i) an excess PbO level in the spinning sol and (ii) a PbO buffer system to establish a well-defined PbO partial pressure during sintering. Dense fibers with a well-defined microstructure and good physical properties were achieved by using an excess PbO content of 4 mol% or higher in combination with a $PbZrO_3$-buffer [20]. On the basis of these results two different excess PbO contents in the spinning sol with z = +0.04 and +0.14 and a $PbZrO_3$ buffer system were chosen for the investigations in the system PZT–SrKNb. Optimum sintering parameters for the PZT/SKN fibers have been identified through a variation of the PbO content in the spinning sol and via sintering experiments with different sintering temperatures, respectively. The microstructural development of PZT/SKN fibers is derived via quantitative image analysis while the fiber nanostructure has been investigated through TEM studies. All batches are fully characterized in terms of their di- and ferroelectric properties.

Experimental

Preparation of sol–gel derived PZT/SKN fibers

PZT/SKN fibers were synthesized via a sol–gel process [21] with an oxidic bulk composition given by $0.98(PbO)_{1+z}(Zr_{0.53}Ti_{0.47})O_2$-$0.02Sr(K_{0.25}Nb_{0.75})O_3$ with z = +0.04 and +0.14, respectively. The resulting spinning material has a solid content of 61–62 wt.%. The spinning material was melted and extruded to fibers with diameters between 25 and 35 μm. A more detailed description of the manufacturing steps is presented elsewhere [20–22]. The fibers were pyrolyzed in two steps (300 °C, 600 °C) to prevent cracking during the removal of the organic residuals [7].

The pyrolyzed fibers were sintered in closed alumina crucibles at 900, 950, 1000, 1050 and 1100 °C, respectively. The heating rate was 1.25 K/min for all sintering experiments; the sintering time was 5 h. The cooling rate was corresponding to the furnace characteristics. For controlling the PbO partial pressure during sintering, $PbZrO_3$ (Chempur) was employed as a standard PbO buffer system, due to the results from experiments conducted on undoped fibers [20].

Composite preparation

For the ferroelectric characterization 1–3 composites with fiber contents of 20–30 vol.% were prepared by aligning fibers parallel and infiltrating them with an epoxy resin. The fiber composites were diced perpendicular to the fiber orientation into thin discs, grounded and polished down to a thickness of about 500 μm. For the microstructural and ferroelectric characterization gold electrodes were sputtered onto the surfaces of the samples (SCD 040, Balzer).\

Microstructural characterization of the fibers

The chemical composition of the fibers was characterized by microprobe analysis (CAMECA SX 50). Phase analysis of the sintered fibers was conducted with powder X-ray diffractometry (Philips 1710). Scanning electron microscopy (SEM) (Hitachi S-800) was carried out on fibers and 1–3 composites. The residual porosity and the grain size distribution of the fibers were derived from polished and chemical etched composite surfaces via quantitative image analysis.

A Philips Tecnai F 30 transmission electron microscope operating at 300 kV acceleration voltage was employed for analysis of the nanoscale microstructure of PZT/SKN fibers. The preparation of TEM cross-section specimens [23] of PZT/SKN fibers via Argon-ion beam thinning was severely impaired. As the main reasons a non-uniform thinning behavior of the perovskite phase(s), percolation of nanopores and local amorphization of PZT/SKN material were observed due to radiation damage during Argon ion beam bombardment. This problem was bypassed by utilizing crushed fiber grain suspensions deposited on a holycarbon film; these suspensions worked sufficiently well for conventional transmission electron microscopy including selected area diffraction and small probe microanalysis. For future work TEM specimen preparation will be performed via focused-ion-beam (FIB) sectioning.

Ferroelectric and electromechanical testing

For the calculation of the dielectric properties of the fibers, the capacitances of 1–3 fiber-composites were measured. The dielectric permittivity ε_r and dielectric loss tan δ were estimated from measurements at frequencies of 1, 10, 100 kHz and 1 MHz. First ferroelectric measurements were carried out with a simple current-voltage converter.

Results and discussion

Pyrolyzed PZT/SKN fibers: microstructure and phase content

All pyrolyzed PZT/SKN fibers (z = +0.04 and +0.14) show a typical core-shell structure (Fig. 1). The grains in the

outer region form a dense shell with grain sizes in the range of 0.5 μm (arrows in Fig. 1), whereas the core region consists of fine-grained agglomerates with grains sizes between 100 and 150 nm and shows high porosity.

For both pyrolyzed fiber batches small variations of the contents of PbO, ZrO_2, and TiO_2 across the fiber diameter were found via microprobe analysis (not shown here). These variations were within the statistical data scattering of typically 2–3 wt.% and could not be correlated with the observed core-shell-mesostructure of the fibers.

Phase analysis via X-ray diffraction (Fig. 2) showed, that for both pyrolyzed fiber batches no crystalline secondary phases (e.g. PbO, ZrO_2 or pyrochlore), were observed within the detection limit (Fig. 2).

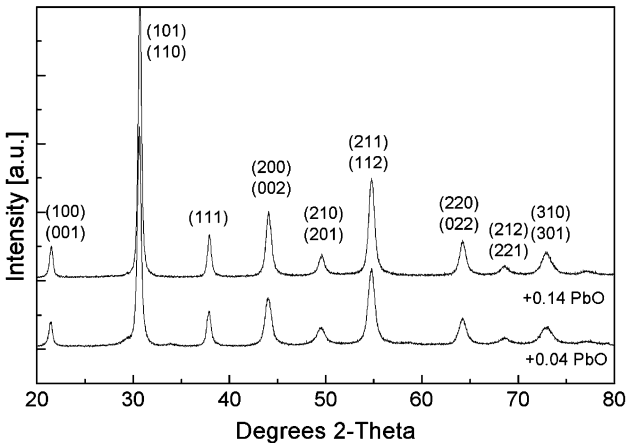

Fig. 2 XRD diffractograms of pyrolyzed PZT fibers at 600 °C with different PbO contents of $z = +0.04$ and $z = +0.14$ in the spinning sol. All two fiber batches consist of perovskite phase, devoid of crystalline secondary phases

Sintered PZT/SKN fibers: sintering temperature variations

Phase content of sintered PZT/SKN fibers

After sintering at 900, 950, 1000, 1050 or 1100 °C, all sintered fibers showed pure PZT in the XRD diffractograms, independently of the PbO-content in the spinning sol ($z = +0.04$ and $+0.14$) or the sintering temperature (Fig. 3). Within the detection limit of the diffractometer, no crystalline secondary phases such as ZrO_2 or PbO could be observed. For samples sintered at 900 °C the relatively broad (200)/(002)- and (310)/(301)-peaks suggest the coexistence of both, the rhombohedral and the tetragonal perovskite phase, as one would expect for stoichiometries close to the morphotropic phase transition. These broad peaks were found for all chosen PbO-contents in the spinning sol.

In contrast, diffractograms of fibers sintered at higher temperatures showed a pronounced splitting of (200)/(002)-, (210)/(201)-, (220)/(022)- and (310)/(301)-interferences with increasing sintering temperature, which can be attributed to a relative increase of the tetragonal $PbTiO_3$-rich phase in the PZT/SKN solid solution. It should be noted that this change in the phase content is not connected with an overall variation of the chemical composition of the samples. Measurements of the chemical composition via ICP-AES analysis revealed that all samples showed the established Zr/Ti-ratio of 53/47 mole% and an excess PbO-level of 5 mole% compared to the nominal PZT composition. Even after a sintering step at 1100 °C for 5 h an excess PbO-level of 4 mole% was observed.

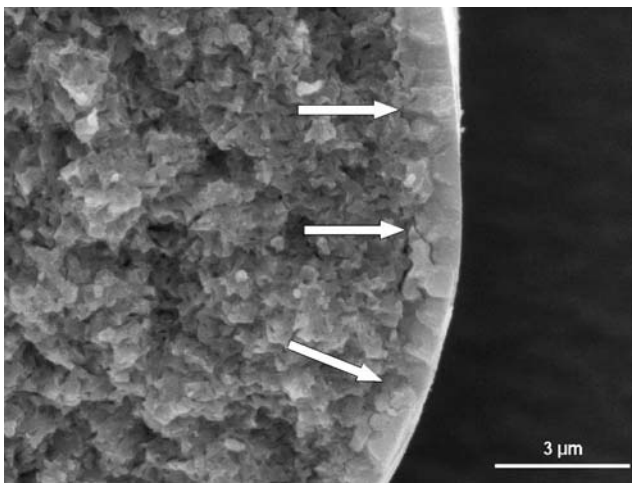

Fig. 1 Microstructure of pyrolyzed PZT fiber at 600 °C with an excess PbO content of $z = +0.04$ in the spinning sol showing the typical core/shell mesostructure

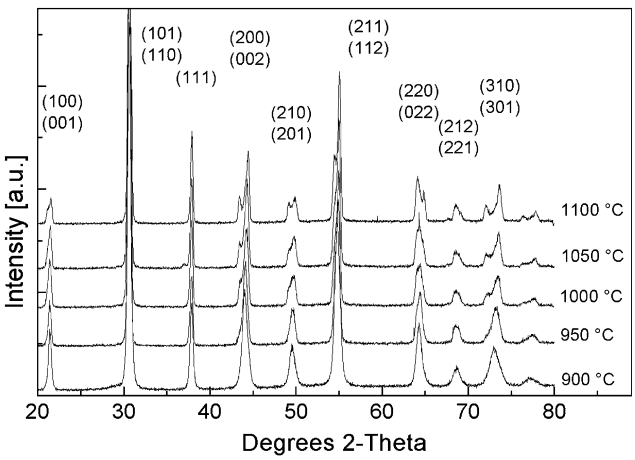

Fig. 3 XRD diffractograms of PZT fibers sintered at different temperatures between 900 and 1100 °C for 5 h. No secondary phases were found

These observations indicate that the increase of the tetragonal, $PbTiO_3$-rich phase is not connected with a decrease of the ZrO_2 level in the PZT crystals due to a PbO-deficiency and the occurrence of unreacted ZrO_2 caused by the evaporation of PbO at the high sintering temperatures. Additionally microprobe analysis profiles across the fiber diameter revealed only small variations of the PbO, the ZrO_2, and the TiO_2 content, which cannot be correlated with an inhomogeneous composition in µm scale.

The apparently increase of the tetragonal phase is in good agreement with results found by other workers, but in most cases no explanation was proposed [19, 24, 25]. Only Fernandes et al. [24] assumed that this could be a consequence of a particle size effect, with the tetragonal phase being favored at larger particle size.

SEM investigations of sintered PZT/SKN fibers

As depicted exemplary in Fig. 4a fibers with a moderate ($z = +0.04$) as well as with a high excess-PbO level up to $z = +0.14$ and sintered at 900 °C for 5 h exhibit a similar gross microstructure consisting of a dense shell and a porous core. This core-shell mesostructure corresponds to that of the pyrolyzed fibers (Fig. 1) indicating that independent from the excess-PbO level the pre-established microstructure from the pyrolysis step cannot be overcome during sintering at 900 °C.

The porous core consists of rounded grains of about 0.2–0.5 µm in size, the grains are connected by sintering necks. The porosity varies between 17 and 19 vol.% for fibers with $z = +0.04$ and between 12 and 15 vol.% for fibers with the higher excess-PbO level of $z = +0.14$.

In contrast, all fiber batches ($z = +0.04$ and $+0.14$) sintered at temperatures above 900 °C achieved full densification independent from the excess-PbO content in the spinning sol. No core-shell effects were observed, indicating that the sintering mechanisms at higher temperatures were strong enough to overcome the pre-established microstructure after pyrolysis and to cause dense fibers with large grain sizes (Fig. 4b, c). Determining the fiber porosity and the average grain size it was found, that the average grain size of the polyhedral shaped grains scales with the sintering temperature. The porosity is lower than about 1 vol.% independent from the PbO content in the spinning sol. For fibers sintered at 950 °C an average grain size between 2 and 3 µm was found within a monomodal grain size distribution, whereas fibers sintered at 1000 °C exhibit average grain sizes between 4 and 5 µm. Sintering at 1050 °C results in grain sizes in the range of 6 and 8 µm. Highest values up to 10 µm were obtained at 1100 °C. All these grains are well faceted, 120° dihedral angles are commonly observed in the grain boundary network, giving evidence that the sintering time is long enough to establish equilibrium conditions in the microstructure.

On the fiber surfaces the equiaxed grain morphology introduces a pillow-like fiber surface structure characterized by networks of 120° dihedral angles (Fig. 5a). Only little porosity could be found, intergranular defects such as cracks and pores have not been detected.

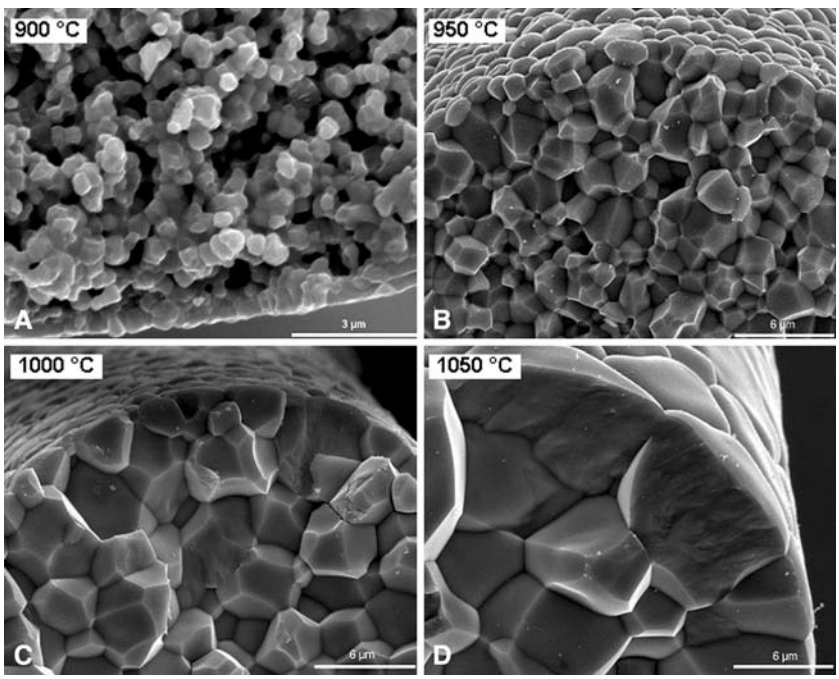

Fig. 4 Fracture surfaces of sintered PZT fibers: (**a**) sintering temperature 900 °C; (**b**) 950 °C; (**c**) 1000 °C; (**d**) 1050 °C. Fibers sintered at 900 °C exhibiting a composite mesostructure consisting of a dense shell and a porous core built of 0.5 µm sized PZT grains. In contrast fibers sintered above 900 °C were fully densified devoid of a core/shell mesostructure. The grain sizes increases with increasing sintering temperature

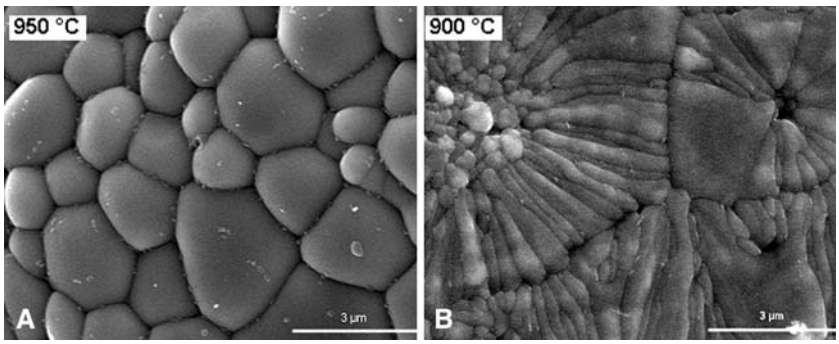

Fig. 5 Fiber surfaces from samples sintered at 900 and 950 °C respectively. Surfaces from samples sintered at 950 °C exhibits a pillow-like surface structure whereas the surface from samples sintered at 900 °C shows a microstructure of rosetted aggregates formed by small grains surrounded by elongated ones

In contrast to the fibers described above a bimodal grain size distribution with two maxima, one between 2 and 3 µm and another at 0.5 µm was obtained from surfaces of fibers sintered at 900 °C. Typical for the microstructure on the fiber surfaces are rosetted aggregates, formed by small grains and surrounded by elongated coarser grains (Fig. 5b).

As expected, fiber fracture surface structures vary significantly with the sintering temperature but not with the PbO-content in the spinning sol. Fibers sintered at temperatures $\leq$ 1000 °C are characterized consistently by an intercrystalline fracture mode, while fibers fired higher than 1000 °C show a mixed mode behavior with transcrystalline fractures of up to 50%. Most transcrystalline fractures were found for fibers with large grain sizes as well as in the outer region of the fibers.

TEM investigations of PZT/SKN fibers with varied sintering temperatures

The TEM results corroborated the general microstructural features of sintered PZT/SKN fibers as derived from XRD and SEM investigations. The PZT/SKN grains are free of pores and form a homogenous two-phase (F_t, F_r) perovskite.

Within the given limitation in TEM specimen preparation, Z-contrast imaging of PZT/SKN fiber suspensions with a high-angle annular dark field (HAADF) detector as well as elemental profiling across individual PZT/SKN grains performed in STEM mode did not reveal compositional gradients. No crystalline secondary phases could be observed at triple grain junctions. Due to the lack of structural integrity of the TEM specimens available, segregations of the dopants Sr, K and Nb at grain boundaries was difficult to verify experimentally.

The fiber batches sintered at 950 °C or higher exhibited an intergranular non-crystalline PbO-rich secondary phase (Fig. 6). Small probe microanalysis from the non-crystalline phase showed substantial Si and Pb concentrations along with various amounts of Al and Fe impurities. Via ICP analysis the origin of these impurities could be traced

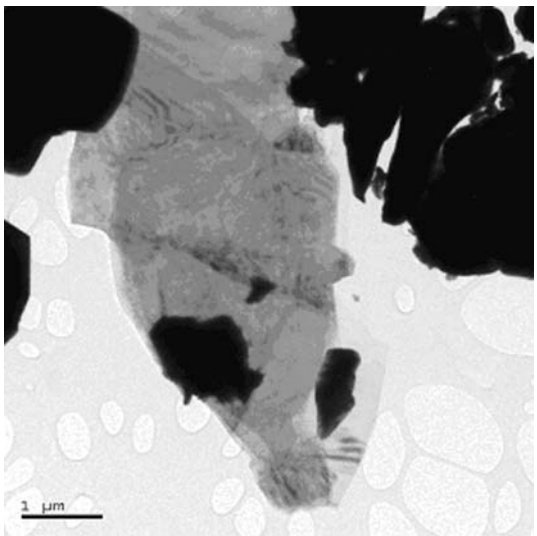

Fig. 6 Multigrain junction in a PZT/SKN fiber (crushed grain suspension, TEM BF) displaying a non-crystalline phase with Si, Al, Ca and Fe impurities (verified via small probe microanalysis)

to intrinsic impurities of the precursors employed for spinning sol synthesis. Measurements of the Zirconium n-propoxide (70% solution in propanol) yielded 0.3 wt.% Al_2O_3 and 0.1 wt.% Fe_2O_3, while in Titanium ethoxide 0.6 wt.% SiO_2 and 0.1 wt.% Fe_2O_3 could be analyzed. HREM images taken from several sufficiently thin areas did reveal nanocrystalline PbO particles embedded in an amorphous phase. Minor phases like m-ZrO_2 as expected from the increased splitting of (200)/(002)-, (210)/(201)-, (220)/(022)- and (310)/(301)-interferences of fibers sintered at higher temperatures could not be observed.

The microstructural change of PZT/SKN fibers upon the small increase of the sintering temperature from 900 to 950 °C is considered due to a change of the prevalent sintering mechanism. At 900 °C, densification of all fiber batches, independently of their PbO-content in the spinning sol, seemed to be controlled by solid state sintering. The common rationale for fine-grained PZT/SKN microstructures is the enrichment of soft dopants at the grain boundaries acting as grain growth inhibitors [26–29]. For

fibers sintered above 900 °C however, the PbO-bearing non-crystalline phase identified at triple grain junctions strongly suggested that in the elevated temperature regime densification is promoted by a liquid-phase sintering mechanism similar to observations from mixed oxide PZT systems [9–12, 20, 27, 30]. This is an interesting finding considering the fact that in undoped PZT systems the sintering mechanism at temperatures in the range of 900 and 950 °C—melting point of pure PbO 884 °C—is primarily controlled by the excess PbO content and not as much by the sintering temperature. For the PZT/SKN system it cannot be ruled out that the formation of a liquid phase may be simply related to the relatively high dopant content and impurity content of the precursors employed for spinning sol synthesis. Additional research is underway to clarify this issue.

Dielectric properties

For the calculation of the dielectric properties of the fibers, the capacitances of 1–3 fiber-composites were measured. No composites could be prepared from fibers with an excess PbO content of $z = +0.04$ sintered at 1100 °C and from all fibers with an excess PbO-level of $z = +0.14$, due to fiber fracture during composite preparation.

In Fig. 7 the ε_r values of the unpoled fibers with $z = +0.04$ are depicted as a function of the sintering temperature in comparison with the average grain size. With increasing sintering temperature up to 1000 °C an increase of the ε_r values from 650 up to 950 is observed. This dependence between the sintering temperature and the ε_r-values agrees well with the increase of the medial grain size with rising sintering temperature, which was observed by SEM investigations. In contrast to this a scarped decrease of the ε_r was observed for fibers sintered at 1050 °C showing ε_r-values of 550 although a further increase of the grain size could be observed. This decrease of the ε_r-values might be explained by the increase of the tetragonal, $PbTiO_3$-rich phase in the PZT/SKN solid solution, which usually is accompanied by a decrease of the dielectric permittivity.

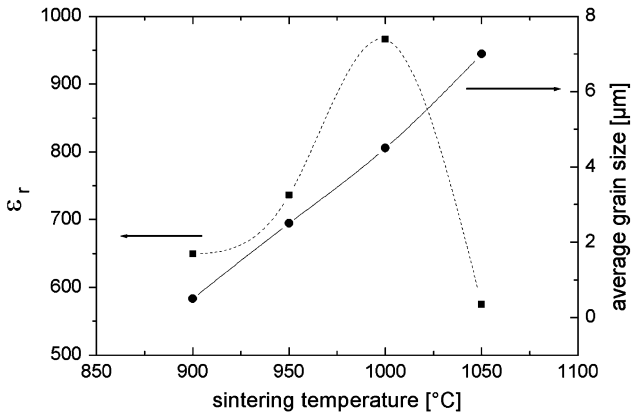

Fig. 7 Dielectric permittivity ε_r correlated with the average grain sizes of unpoled PZT/SKN fibers as a function of the sintering temperature

Ferroelectric properties

Hysteresis measurements were carried out at a frequency of 50 Hz. In Fig. 8 typical hysteresis loops with increasing applied field strength are shown. For all samples a non-linear response in the hysteresis loops could be observed at an electric field strength of 1 V/µm. This is typical for substituted or soft-doped PZT ceramics. With rising electrical field strength a strong increase of the remanent and maximal polarization and of the coercivity could be measured. Characteristically for all samples is the small ratio of the maximum and the remanent polarization, leading to a scarped curve progression at the coercivity. The characteristic ferroelectric properties from these measurements at a field strength of 5 V/µm after 10,000 cycles were summarized in Table 1. As can be seen from the values in Table 1 a strong increase of the remanent and maximum polarization with increasing sintering temperature could be observed, which is in good agreement with the observation from measurements of the dielectric properties. Again a strong decrease of the values of the remanent and maximum polarization could be found for fibers sintered at 1050 °C. The coercivity of these samples is in the range of 2.1 V/µm in contrast to fibers sintered at lower temperatures with values of about 1.9 V/µm. A feasible explanation for this effect is again the shift in the phase content.

Conclusions

Sol–gel derived PZT fibers in the solid solution system PZT/SKN with a Zr/Ti content at the morphotropic phase transition (53/47) have been evaluated. The batch composition was defined by $0.98(PbO)_{1+z}(Zr_{0.53}Ti_{0.47})O_2$-$0.02Sr(K_{0.25}Nb_{0.75})O_3$ with the parameter z specifying the excess PbO content in the spinning sol. By varying both, the excess PbO content, i.e. $z = +0.04$ and $z = +0.14$, and the sintering temperatures between 900 and 1100 °C, fibers with a fully densified, homogeneous PZT microstructure could be achieved. All batches consisted of single-phase perowskite phase, devoid of crystalline secondary phases. Fiber diameters were typically of the order of 20 µm.

With increasing sintering temperatures a strong increase of the grain size accompanied by a decrease in porosity was found. Fibers sintered at 900 °C exhibited a narrow grain

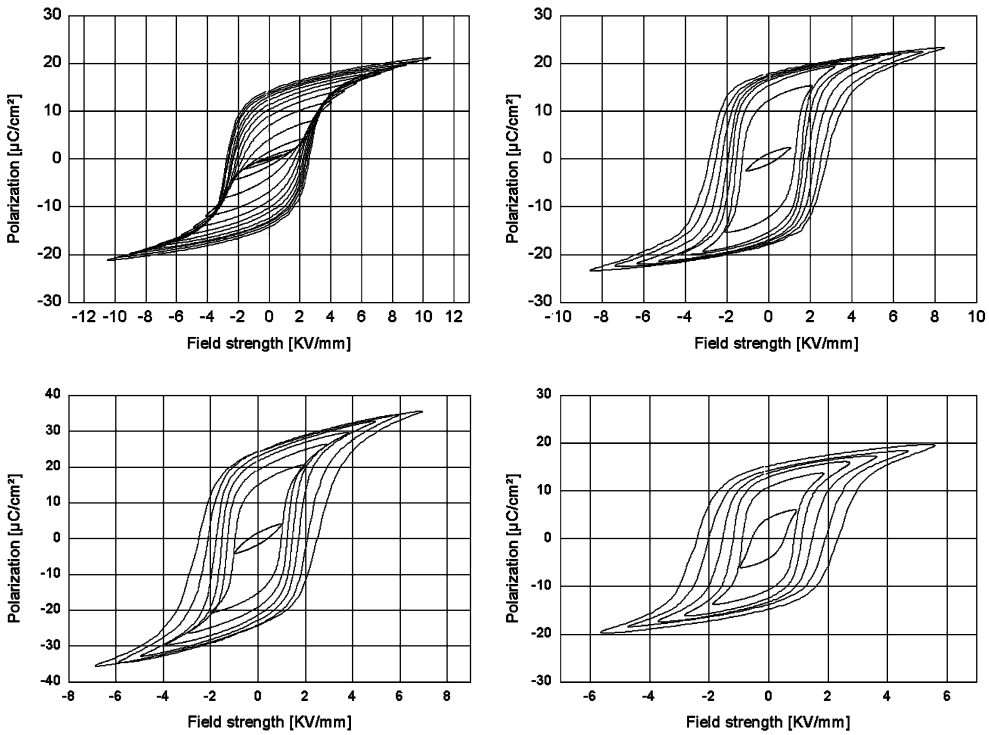

Fig. 8 Ferroelectric hysteresis loops of PZT/SKN fibers with an excess PbO content of $z = +0.04$ in the spinning sol: The measurements were carried out for different applied field strengths after 10,000 cycles: Sintering temperature of the fibers: (**a**) 900 °C; (**b**) 950 °C; (**c**) 1000 °C; (**d**) 1050 °C

Table 1 Characteristic ferroelectric properties of PZT fibers with different PbO contents in the spinning sol

	Sintering temperature of PZT/SKN fibers with $z = +0.04$			
	900 °C	950 °C	1000 °C	1050 °C
Coercivity E_c (V/µm)	1.9 ± 0.2	1.9 ± 0.2	1.9 ± 0.3	2.1 ± 0.2
Max. polarization P_{max} ($\mu C/cm^2$)	15 ± 2	21 ± 2	34 ± 2	19 ± 2
Rem. Polarization P_{rem} ($\mu C/cm^2$)	9 ± 1	17 ± 1	22 ± 1	14 ± 1

size distribution centered at approx. 0.5 µm. Porosity was between 17 and 19 vol.% for fibers with $z = +0.04$ which could be further reduced to 12–15 vol.% for fibers with a higher excess PbO level of $z = +0.14$. For a sintering temperature of 1100 °C a strong increase of the grain sizes up to 10 µm was obtained.

Microstructural data suggest that below 900 °C densification of PZT/SKN fibers is controlled by solid state sintering while liquid phase sintering becomes the dominant densification mechanism above 900 °C.

The dielectric and ferroelectric properties of the fibers vary significantly with the average grain size; the best performance was obtained for fibers sintered at 1000 °C. These fibers exhibit dielectric permittivity in the range of 1000 and remanent polarization values of 22 $\mu C/cm^2$ with coercivities at 1.9 V/µm. Fibers sintered at higher temperatures showed a decrease of the remanent and maximal polarization as well as in the dielectric ε_r values combined with an increasing coercivity.

Acknowledgements This research has been supported by the Deutsche Forschungsgemeinschaft (DFG), SPP 734 through grants Br 923/4 and Mu 720/16. The stimulating discussions with the mentors of SPP 734, Prof. Thomann and Prof. Härdtl as well as B. Hildmann, DLR, are gratefully acknowledged. The authors appreciate the TEM preparation work performed by G. Paul, DLR.

References

1. Uchino K (1998) Acta Mater 46:3745
2. Newnham RE (1997) MRS Bull 5:20
3. Newnham RE, Ruschau GR (1991) J Am Ceram Soc 74(3):463
4. Haertling GH (1999) J Am Ceram Soc 82(4):797
5. Safari A, Janas VF, Bandyopadhyay A (1997) Ceram Process 43(11A):2849
6. Park YI, Miyayama M (1999) Key Eng Mater 157–158:33–40
7. Scholz H, Watzka W, Sporn D, Seffner L, Schönecker A (1995) In: Proceedings of ICCM-10, Whistler, B.C., Canada, pp IV-481–IV-488
8. Janas VF, Safari A (1995) J Am Ceram Soc 78(11):2945
9. James AD, Messer PF (1978) J Br Ceram Soc 77:152
10. Kingon A, Clark B (1983) J Am Ceram Soc 66(4):253
11. Kingon A, Clark B (1983) J Am Ceram Soc 66(4):256
12. Snow GS (1973) J Am Ceram Soc 56(2):91
13. Klicker KA, Biggers JV, Newnham RE (1981) J Am Ceram Soc 64(1):5
14. Savakus HP, Klicker KA, Newnham RE (1981) Mater Res Bull 16:677
15. Lubitz RE, Wolff A, Preu G, Schulmeyer B (1993) Ferroelectrics 133(1–4):21

16. Gentilman RL, Fiore DF, Pham HT, French KW, Bowen LJ (1994) In: Bhalla AS, Nair KM, Lloyd IK, Yanagida H, Payne DA (eds) Ferroic materials: design, preparation and characteristics. Amer. Cer. Soc., 43, p 239
17. Steinhausen R, Hauke T, Seifert W, Beige H, Watzka W, Seifert S, Sporn D, Starke S, Schönecker A (1999) J Eur Ceram Soc 19:1289
18. Helke G, Schönecker A, Obenaus P, Keitel U, Seffner L, Scholehwar T, Lange U (2000) Ferroelectrics 1:435
19. Helke G, Seifert S, Cho S-J (1999) J Eur Ceram Soc 19:1265
20. Hansch R, Seifert S, Braue W, Sporn D, Müller G (2004) J Eur Ceram Soc 24:2485
21. Glaubitt W, Watzka W, Scholz H, Sporn D (1997) J Sol-Gel Sci Technol 8:29
22. Helbig J, Glaubitt W, Spaniol H, Vierhaus P, Lange U, Hansch R, Watzka W, Sporn D (2003) Smart Mater Struct 12:987
23. Williams DB, Carter CB (1996) Transmission electron microscopy: a textbook for materials science. Plenum Press, New York, p 750
24. Fernandes JC, Hall DA, Cockburn MR, Greaves GN (1995) Nucl Instr Methods Phys Res B97:137
25. Mabud SA (1980) J Appl Cryst 13:211
26. Atkin RB, Fulrath RM (1971) J Am Ceram Soc 54(5):265
27. Hammer M, Hoffmann MJ (1998) J Am Ceram Soc 81(12): 3277
28. Wen J, Hellebrand H, Cramer D, Lubitz K, Tomandl G (1994) In: Proc. Electroceramics IV. Waser R (ed) Verlag der Augustinusbuchhaudlung, Aachen, vol 1, p 247
29. Yoshikawa S, Selvaraj U, Moses P, Jiang Q, Shrout T (1994) Ferroelectrics 154:325
30. Akbas M, Michael A, McCoy A, Lee WE (1995) J Am Ceram Soc 78(9):2417